

University of Dundee

Identification of Endogenous Adenomatous Polyposis Coli Interaction Partners and - Catenin-Independent Targets by Proteomics

Popow, Olesja; Paulo, Joao A.; Tatham, Michael; Volk, Melanie; Rojas-Fernandez, Alejandro; Loyer, Nicolas

Published in:
Molecular Cancer Research

DOI:
[10.1158/1541-7786.MCR-18-1154](https://doi.org/10.1158/1541-7786.MCR-18-1154)

Publication date:
2019

Document Version
Peer reviewed version

[Link to publication in Discovery Research Portal](#)

Citation for published version (APA):

Popow, O., Paulo, J. A., Tatham, M., Volk, M., Rojas-Fernandez, A., Loyer, N., Newton, I., Januschke, J., Haigis, K. M., & Nathke, I. (2019). Identification of Endogenous Adenomatous Polyposis Coli Interaction Partners and - Catenin-Independent Targets by Proteomics. *Molecular Cancer Research*, 17(9), 1828-1841. <https://doi.org/10.1158/1541-7786.MCR-18-1154>

General rights

Copyright and moral rights for the publications made accessible in Discovery Research Portal are retained by the authors and/or other copyright owners and it is a condition of accessing publications that users recognise and abide by the legal requirements associated with these rights.

- Users may download and print one copy of any publication from Discovery Research Portal for the purpose of private study or research.
- You may not further distribute the material or use it for any profit-making activity or commercial gain.
- You may freely distribute the URL identifying the publication in the public portal.

Take down policy

If you believe that this document breaches copyright please contact us providing details, and we will remove access to the work immediately and investigate your claim.

1 **Identification of endogenous Adenomatous polyposis coli interaction partners**
2 **and β -catenin-independent targets by proteomics**

3

4 Olesja Popow^{1,2}, João A. Paulo², Michael H. Tatham³, Melanie S. Volk⁵, Alejandro
5 Rojas-Fernandez⁴, Nicolas Loyer⁵, Ian P. Newton⁵, Jens Januschke⁵, Kevin M.
6 Haigis^{1,6}, Inke Näthke^{5*}

7

8 ¹Cancer Research Institute and Department of Medicine, Beth Israel Deaconess
9 Medical Center, Boston, MA 02215, United States

10 ²Department of Cell Biology, Harvard Medical School, Boston, MA 02115, United States

11 ³Centre for Gene Regulation and Expression, School of Life Sciences, University of
12 Dundee, Dundee, DD1 5EH, Scotland UK

13 ⁴Center for Interdisciplinary Studies on the Nervous System (CISNe) and Institute of
14 Medicine, Universidad Austral de Chile, Valdivia, Chile

15 ⁵Cell and Developmental Biology, School of Life Sciences, University of Dundee,
16 Dundee, DD1 5EH, Scotland UK

17 ⁶Harvard Digestive Disease Center, Harvard Medical School, Boston, MA 02215, United
18 States

19

20 **Running title:** The APC interactome and its β -catenin-independent targets.

21

22 **Keywords:** Adenomatous polyposis coli, destruction complex, colorectal cancer,
23 proteomics, Misshapen-like kinase 1.

24

25 **Financial Support:** Olesja Popow - CRUK PhD fellowship, João A. Paulo - NIH/NIDDK
26 grant K01 DK098285, Michael H. Tatham – supported by CRUK program grant to R.
27 Hay, Alejandro Rojas-Fernandez - FONDECYT 11150532 and PAI79150075, Nicolas
28 Loyer and Jens Januschke - Sir Henry Dale fellowship (Wellcome/Royal Society:
29 100031Z/12/Z), Kevin M. Haigis - NIH/NCI grant U01CA199252, Ian P. Newton and
30 Inke Näthke – CRUK program grant to Inke Näthke.

31

32 **Corresponding author:** Inke Näthke, Cell and Developmental Biology, University of
33 Dundee, Dow Street, Dundee, DD15EH, Scotland UK. Phone: +44-1382-385821; E-
34 Mail: i.s.nathke@dundee.ac.uk

35

36 Conflict of interest disclosure: The authors declare no potential conflicts of interest.

37

38 Word count: 6522

39 1 Table, 6 Figures, 6 Supplementary Figures, 2 Supplementary Tables

40

41 **Abstract**

42 *Adenomatous Polyposis Coli (APC)* is the most frequently mutated gene in colorectal
43 cancer. APC negatively regulates the Wnt signaling pathway by promoting the
44 degradation of β -catenin, but the extent to which APC exerts Wnt/ β -catenin-independent
45 tumor suppressive activity is unclear. To identify interaction partners and β -catenin-
46 independent targets of endogenous, full-length APC, we applied label-free and
47 multiplexed TMT mass spectrometry. Affinity enrichment-mass spectrometry identified
48 more than 150 previously unidentified APC interaction partners. Moreover, our global
49 proteomic analysis revealed that roughly half of the protein expression changes that
50 occur in response to APC loss are independent of β -catenin. Combining these two
51 analyses, we identified Misshapen-like kinase 1 (MINK1) as a putative substrate of an
52 APC-containing destruction complex. We validated the interaction between endogenous
53 MINK1 and APC and further confirmed the negative – and β -catenin-independent –
54 regulation of MINK1 by APC. Increased Mink1/Msn levels were also observed in mouse
55 intestinal tissue and *Drosophila* follicular cells expressing mutant *Apc/APC* when
56 compared to wild-type tissue/cells. Collectively, our results highlight the extent and
57 importance of Wnt-independent APC functions in epithelial biology and disease.
58 Implications: The tumor suppressive function of APC - the most frequently mutated
59 gene in colorectal cancer – is mainly attributed to its role in β -catenin/Wnt signaling. Our
60 study substantially expands the list of APC interaction partners and reveals that
61 approximately half of the changes in the cellular proteome induced by loss of APC
62 function are mediated by β -catenin-independent mechanisms.

63

64

65 **Introduction**

66 Mutations in *Adenomatous Polyposis Coli* (*APC*) are a frequent (> 80%) and early event
67 in the development of sporadic colorectal cancer (1, 2). Germline mutations in *APC* also
68 form the genetic basis of Familial Adenomatous Polyposis (FAP), an inherited form of
69 the disease that is characterized by hundreds of colorectal polyps that progress to
70 cancerous lesions if left untreated (3). This makes a comprehensive understanding of
71 the normal interactions and functions of *APC* crucial for effectively targeting *APC* mutant
72 cells.

73 The tumor suppressive function of *APC* has been mainly attributed to its role in
74 Wnt signaling. In conjunction with Axin, *APC* acts as a scaffold for the β -catenin
75 destruction complex, thereby limiting the transcription of pro-proliferative β -catenin
76 target genes in the absence of Wnt ligands (4). The vast majority of *APC* mutations
77 result in the translation of a truncated protein and consequent deregulation of Wnt
78 signaling (1, 2). Nevertheless, Wnt-independent roles of *APC* likely also contribute to its
79 function as a tumor suppressor. This is exemplified by the rare detection of mutations in
80 other Wnt signaling components, including β -catenin, in colorectal cancer (5). Although
81 deletion of *Apc* in the intestinal epithelium in mice phenocopies homozygous truncation
82 mutations, it leads to more rapid onset of tumors despite lower levels of Wnt activation
83 (6). It thus emerges that loss of wild-type (WT) *APC* confers additional advantages to
84 cells beyond β -catenin-mediated proliferation, but the extend of *APC*'s Wnt-independent
85 functions is unclear.

86 A variety of proteins have been described to interact with APC in addition to β -
87 catenin destruction complex components (7). However, proteome-wide studies of APC-
88 binding proteins are limited to interactome and yeast-two-hybrid experiments with
89 overexpressed, tagged and/or fragments of APC (8-11). Using tagged APC in
90 interaction studies is problematic because the C-terminal PDZ-binding domain must
91 remain free to interact with other proteins (12). Similarly, the N-terminal oligomerization
92 domains rely on coiled-coil formation and may be compromised by N-terminal tags (13).
93 To overcome these limitations, we used label-free affinity-enrichment mass
94 spectrometry (AE-MS) to identify a more comprehensive set of interacting partners of
95 endogenous, non-tagged APC. Furthermore, we applied an untargeted global approach
96 using tandem mass tag (TMT)-based and label-free MS to identify proteins that are
97 regulated by APC in their abundance. These two data sets provide a unique resource
98 for the exploration of Wnt/ β -catenin-dependent and independent functions of APC. In
99 addition, we could identify potential targets of APC-containing destruction complexes by
100 combining our data on APC-interacting and APC-regulated proteins (Figure 1A). While
101 no direct evidence for the assembly of such complexes by APC exists, other
102 components of the β -catenin destruction complex, such as GSK-3 β and SCF ^{β -TrCP}, are
103 known to have many targets (14, 15). We thus hypothesized that APC may directly
104 regulate the abundance of other proteins in addition to β -catenin.

105

106 **Materials and Methods**

107 Cell Culture

108 Colo320, HeLa, and SW480 cells were obtained from the American Type Culture
109 Collection. U2OS cells were obtained from CRUK. The HCT116-Haβ92 cell line was a
110 kind gift of Todd Waldman, HeLa SEC-C and U2OS SEC-C parental cell lines were a
111 kind gift of Ron Hay, the U2OS Flp-In™ T-Rex™ host cell line was a kind gift of Carol
112 MacKintosh. Cells were grown at 37 °C and 5% CO₂ in Dulbecco's modified eagle
113 medium (DMEM) with 10% fetal bovine serum, 50 U/mL penicillin/streptomycin, and 1%
114 v/v non-essential amino acids (all Thermo Fisher Scientific). HeLa SEC-C, U2OS SEC-
115 C, U2OS Flp-In™ T-Rex™ and cell lines generated from these were grown as
116 described above, with the addition of 100 µg/mL Hygromycin B and 15 µg/mL Blasticidin
117 to the cell culture medium. Cells were culture for a maximum of 20 passages after
118 thawing. Cells were tested for mycoplasma contamination every 6 months using
119 MycoAlert™ (Lonza, Cat# LT-07-418).

120

121 Generation of cell lines

122 *U2OS SEC-C MINK1 knockout cell lines*

123 Analysis of the N-terminal coding region of *MINK1* (ensembl ENSG00000141503)
124 predicted potential gRNAs with high target affinity, high efficiency and low off-target
125 scores with binding sites in exon 1 and exon 2 using CRISPR Design. We used the best
126 scoring gMINK1 target site in exon 1 (CGGACAGGTCGATGTCGTCC [AGG]) with a
127 score of 95 and 12 predicted off-target sites in other genes. The gRNA sequence was
128 cloned into pBabeD pU6 and sequence-verified. U2OS cells stably expressing Cas9
129 (U2OS SEC-C) were co-transfected with 3 µg pBabeD pU6 gMINK1 using
130 Lipofectamine 2000 according to the manufacturer's instructions (Thermo Fisher

131 Scientific, Cat# 11668027). Cells were grown in DMEM supplemented with 10% FBS, 2
132 mM L-glutamine, and 100 $\mu\text{g}/\text{mL}$ NormocinTM (InvivoGen, Cat# ant-nr-1). After 12 h,
133 medium was replaced with fresh medium with 4 $\mu\text{g}/\text{mL}$ Puromycin. After 48 h of
134 selection, 2 $\mu\text{g}/\text{mL}$ doxycycline was added to induce Cas9 expression. After 72 h, single
135 cells were sorted with an InfluxTM cell sorter (BD Biosciences) into 96-well plates
136 containing DMEM with 20% FBS, 2 mM L-glutamine, 100 U/mL penicillin, 100 $\mu\text{g}/\text{mL}$
137 streptomycin, and 100 $\mu\text{g}/\text{mL}$ NormocinTM. MINK1 protein expression was screened by
138 western blotting. Genomic DNA of MINK1 KO cells was amplified by PCR and
139 sequenced to confirm the introduction of frameshift mutations.

140 *HeLa SEC-C mNeonGreen-MINK1*

141 The same pBabeD pU6 gMINK1 vector used for the generation of MINK1 knock-out
142 cells was used for the fusion of mNeonGreen to the N-terminus of MINK1 in HeLa SEC-
143 C cells as described previously (16). A donor vector was designed to replace the ATG
144 start codon of *MINK1* with the start codon of an mNeonGreen cDNA cassette, flanked
145 by ~500 bp homology arms. The donor vector was synthesized by GeneArt (Life
146 Technologies). Expression of mNeon-MINK1 in selected and expanded single cell
147 clones was validated by western blotting and microscopy.

148 *U2OS Flp-In T-Rex MINK1-GFP/GFP*

149 Stable cell lines with tetracycline/doxycycline-inducible expression of MINK1-GFP/GFP-
150 MINK1 and GFP, respectively, were generated using the Flp-InTM T-RexTM System
151 according to the manufacturer's instructions (Thermo Fisher Scientific) by transfecting
152 U2OS Flp-InTM T-RexTM host cells with pcDNA5 FRT/TO C-GFP, pcDNA5 FRT/TO

153 MINK1-GFP, or pcDNA5 FRT/TO GFP-MINK1 respectively, and pOG44, a constitutive
154 Flp recombinase expression plasmid.

155

156 Generation of fly lines and mosaic follicular epithelia

157 The YFP-fused, endogenously expressed allele *msn*^{CPT1003908} was recombined with the
158 FRT[82B], *apc1*⁻, *apc2*⁻ chromosome by meiotic recombination. *msn*^{CPT1003908}, FRT[82B],
159 *apc1*⁻, *apc2*⁻ and Hs-*flp* ; Ubi-*PH*^{PLC δ 1}::*RFP* ; FRT[82B], Ubi-*nls*::*RFP* flies were crossed
160 and *apc1*⁻, *apc2*⁻ mutant clones in follicular epithelial cells in the resulting progeny were
161 induced by a 2 hour, 37 °C heat-shock at a late (starting to pigment) pupal stage.

162

163 Transfections

164 For siRNA transfections cells were transfected one day after seeding with siGENOME
165 APC siRNA #1-#3 (Dharmacon, Cat# D-003869-05/06/07), Hs_CTNNB1_5 FlexiTube
166 siRNA (Qiagen, Cat# SI02662478), or siGENOME Non-Targeting siRNA #1
167 (Dharmacon, Cat# D-001210-01-05) using INTERFERin® (Polyplus-Transfection, Cat#
168 409-10) using 72 ng siRNA/T-25 flask. Colo320 cells were transfected twice on two
169 consecutive days. For plasmid transfections cells were transfected one day after
170 seeding with 4 μ g myc-tagged β -catenin constructs (17)/10 cm dish using Fugene® 6
171 Transfection Reagent (Promega, Cat#2691).

172

173 Mice

174 All mice were obtained from The Jackson Laboratory and bred and maintained in
175 accordance with their recommendations under specific pathogen-free conditions in the

176 Biological Resource Unit at the University of Dundee. Compliant with the ARRIVE
177 guidelines the project was approved by the University Ethical Review Committee and
178 authorized by a project license under the UK Home Office Animals (Scientific
179 Procedures) Act 1986.

180

181 Protein and RNA harvest

182 To harvest proteins, cells or cryo-pulverized mouse small intestinal tissue were lysed in
183 50 mM Tris-HCl pH 7.5, 100 mM NaCl, 5 mM EDTA, 5 mM EGTA, 40 mM β -
184 glycerophosphate, 0.5% NP-40, 1 mM sodium fluoride, 0.1 mM sodium orthovanadate,
185 and 10 μ g/mL of each leupeptin, pepstatin A, and chymostatin. Lysates were cleared by
186 centrifugation and supernatants were collected for further processing. Total RNA was
187 isolated using the NucleoSpin[®] RNA II Kit (Machery-Nagel, Cat# 740955.10).

188

189 Immunoprecipitations

190 For APC IPs 40 μ l protein G-sepharose (Sigma-Aldrich, Cat# P-3296) was washed with
191 protein lysis buffer and incubated for 12 h with 80 μ g (for AE-MS)/20-40 μ g (for WB) of
192 ALI-12-28/C-APC 41.1 antibody (both CRUK) or control V5 tag antibody (kind gift of R.
193 Hay) at 4 °C on a rotating wheel. Antibodies were crosslinked to sepharose using
194 bis[sulfosuccinimidyl]suberate (Thermo Fisher Scientific, Cat# 21580). Antibody-
195 crosslinked sepharose was incubated with pooled cell lysates harvested from five 15 cm
196 dishes (AE-MS and validation Co-IPs)/10 mg protein lysate (all other APC Co-IPs) for
197 12 hours at 4 °C on a rotating wheel.

198 For GFP IPs 15 μ l GFP-Trap®_A beads (Chromotek, Cat# gta-100) were washed twice
199 with PBS and twice with protein lysis buffer. Lysates harvested from one 15 cm dish of
200 U2OS Flp-In T-Rex MINK1-GFP/GFP-MINK1/GFP cells grown for two days in media
201 containing 75 ng/mL Tetracycline was incubated with the beads for 4 hours at 4 °C on a
202 rotating wheel.

203 Beads were washed repeatedly with 20 mM Tris-HCl pH 7.5, 150 mM NaCl, 1 mM
204 EDTA, 0.05% Triton X-100, and 5% glycerol (for APC IPs) or protein lysis buffer (for
205 GFP-IPs). Proteins were eluted by boiling with 1.3x NuPAGE™ LDS sample buffer
206 (Thermo Fisher Scientific, Cat# NP0008).

207

208 SDS-PAGE and Western Blotting

209 Protein samples (50 μ g (cell lysates)/100 μ g (tissue lysates) were separated on pre-cast
210 NuPAGE™ 4-12% gradient Bis-Tris polyacrylamide protein gels (Thermo Fisher
211 Scientific, Cat# NP0322/NP0321), transferred to nitrocellulose membrane, and blotted
212 with primary antibodies: anti-ABI2 (Cat# 302-499A, RRID: AB_1966095), anti-GIT1
213 (Cat# 302-101A, RRID: AB_1604200), anti-GIT2 (Cat# 302-103, RRID: AB_1604269),
214 anti-RNF20 (Cat# 300-714A, RRID: AB_533428), anti-hPrp3p (Cat# 302-073A, RRID:
215 AB_1604202), anti-MINK1 (Cat# A302-192A, RRID: AB_1659822), anti-PAK1 (Cat#
216 301-259A, RRID: AB_890620), anti-PDZ-GEF2 (Cat# 301-967A, RRID: AB_1548003),
217 anti-RNF25 (Cat# 303-844A, RRID: AB_2620195; all Bethyl Laboratories); anti-Aurora
218 B (Cat# ab2254, RRID: AB_302923), anti-CASK (Cat# ab99039, RRID: AB_10696957),
219 anti-LATS1 (Cat# ab70562, RRID: AB_2133360; all Abcam); anti-GAPDH (Millipore,
220 Cat# MAB374, RRID: AB_2107445); anti-GFP (Clontech Laboratories, Cat# 632381;

221 RRID: AB_2313808); anti-LSM7 (Cat# 18941-1-AP, RRID: AB_10596483), anti-TBP
222 (Cat#66166-1-Ig, both Proteintech) anti- β -catenin (BD Transduction Laboratories, Cat#
223 610154, RRID: AB_397555); sheep polyclonal anti-GFP (MRC PPU Dundee, S268B);
224 mouse monoclonal anti-APC N-terminus (CRUK, ALI-12-28); rabbit polyclonal anti-APC
225 N-terminus (18); anti- β -catenin (19). Anti-mouse/rabbit Alexa Fluor Plus 800/680-
226 conjugated secondary antibodies (Thermo Fisher Scientific, Cat# A32735, RRID:
227 AB_2633284/Cat# A32730, RRID: AB_2633279/Cat# A32734; RRID:
228 AB_2633283/Cat# A32729, RRID: AB_2633278) were detected and quantified with the
229 Li-Cor Odyssey imaging system and Image Studio Software.

230

231 Immunofluorescence and live imaging

232 *Cells*

233 For immunofluorescence, cells grown on collagen-coated No. 1.5 cover glass were fixed
234 for 10 min with -20 °C methanol, permeabilized using 1% NP40 in PBS for 10 min, and
235 incubated with IF blocking buffer (5% normal goat serum, 2% w/v BSA, 0.1% Triton X-
236 100 in 1x PBS) for 30 min at RT. Cells were washed with 0.2% w/v BSA in 1x PBS, in
237 between steps. Anti-MINK1 antibody (Thermo Fisher Scientific, Cat #PA5-28901, RRID:
238 AB_2546377) was diluted 1:250 in blocking buffer without serum and incubated
239 overnight at 4 °C. After repeated washing, cells were incubated for one hour with
240 20 μ g/mL Hoechst 33342 (Invitrogen, Cat# H3570) and Alexa Fluor® 594 anti-rabbit
241 antibody (Thermo Fisher Scientific, Cat #PA5-28901; RRID: AB_2546377) diluted
242 1:500. Cover slips were mounted onto microscopy slides using 90% glycerol with 0.5%
243 N-propyl gallate. For live imaging, cells were grown on 35 mm glass bottom dishes

244 (ibidi, Cat# 81418-200) in DMEM without phenol red. Images were acquired with an
245 inverted Nikon Eclipse Ti-E fluorescence microscope equipped with a Hamamatsu
246 ORCA-R² digital CCD camera and a Prior Scientific Lumen 200PRO light source, using
247 a Plan Apo 60x NA 1.4 objective lens. Images were acquired with the MetaMorph
248 software (version 7.8.12.0) and without camera binning. 395/25; 480/40; and 545/30
249 excitation and 460/50; 535/50; and 620/60 emission filters were used for Hoechst,
250 mNeonGreen, and Alexa594. Image brightness and contrast was adjusted equally for
251 each image using Fiji software (20).

252 *Drosophila* egg chambers

253 Msn::YFP-expressing, mosaic *apc1*⁻, *apc2*⁻ mutant female flies were dissected 24 hours
254 after hatching. Ovaries dissected in glucose- (1 g/L) and insulin- (0.2 g/L) supplemented
255 Schneider's medium (Lonza, Cat# lz04-351q) in a 35 mm glass bottom dish into
256 individual ovarioles. Imaging was performed on a SP8 confocal microscope (LEICA)
257 equipped with a 63x NA 1.2 water immersion objective within the hour following
258 dissection. The Nls::RFP marker was used to discriminate *apc1*⁻, *apc2*⁻ mutant
259 cells, *apc1*⁺, *apc2*⁺ control cells and *apc1*⁻, *apc2*⁻ / *apc1*⁺, *apc2*⁺ heterozygous control
260 cells. Msn::YFP levels were measured at the interface between cells of the same
261 genotype and, for each egg chamber, normalized to the median value measured at the
262 interfaces between heterozygous control cells.

263

264 Cell adhesion assay

265 96-well plates coated with 10 µg/cm² collagen (Sigma-Aldrich, Cat# 8919) were washed
266 with PBS and incubated for one hour with DMEM + 0.5% bovine serum albumin (BSA)

267 at 37 °C. Cells were detached with 10 mM EDTA in PBS for 10 min at 37 °C, washed
268 twice with DMEM, counted using a Cellometer® Auto T4 bright field cell counter
269 (Nexcelom Bioscience), and diluted to a density of 1×10^5 cells/mL in DMEM + 0.1%
270 BSA. 10,000 cells were added per well and incubated for 1 h at 37 °C. Loosely attached
271 cells were removed by vigorous shaking of the plate for 10 s, and washing with DMEM +
272 0.1% BSA. Adherent cells were fixed with 4% paraformaldehyde for 10 min, washed,
273 and stained for 10 min with 5 mg/mL crystal violet in 2% ethanol. Plates were washed
274 once with water and then dried overnight. Crystal violet stain was solubilized with 200 μ l
275 2% SDS/well for 30 min and diluted 1:4 with water. Absorption was measured at 550 nm
276 using a Synergy H1 Hybrid multi-mode microplate reader (BioTek).

277

278 MTT cell proliferation assay

279 Cells were seeded one day after transfection in 96 cells plates with 1×10^5 cells/well.
280 Viable cells was measured using the TACS® MTT Proliferation Assay Kit (Trevigen,
281 Cat# 4890-25-01 and Cat# 4890-25-02).

282

283 Real Time-quantitative PCR (RT-qPCR)

284 cDNA was synthesized using the qScript™ cDNA Synthesis Kit (Quanta Biosciences,
285 Cat# 95047). RT-qPCR reactions were performed in triplicate using PerfeCTa SYBR®
286 Green FastMix (Quanta Biosciences, Cat# 95072) and a CFX Connect™ Real-Time
287 PCR Detection System (Bio-Rad). C_T values obtained for target genes were normalized
288 to *ACTB* and relative mRNA expression was calculated using the Pfaffl method (21).
289 Primer sequences: *ACTB* forward/reverse –

290 CTGGGAGTGGGTGGAGGC/TCAACTGGTCTCAAGTCAGTG, *AXIN2* forward/reverse:
291 TGGCTATGTCTTTGCACCAG/TGTTTCTTACTGCCACACG, *CTNNB1*
292 forward/reverse: ATGGCTTGAATGAGACTGC/TTCCATCATGGGGTCCATAC,
293 *MINK1* forward/reverse: TCAACCTGCTCATCACCATC/TCCACTTCTGGGTCATTGTG.

294

295 Protein analysis by mass spectrometry

296 For label-free MS analysis Co-IP and complete lysate samples were separated by SDS-
297 PAGE and proteins were visualized by Coomassie Blue staining. Gel lanes were
298 subdivided into three parts – gel regions containing co-eluted antibody chains in Co-IP
299 samples were pooled. In-gel tryptic digestion was performed as described previously
300 (22). Peptides solubilized in 1% FA were analyzed by LC-MS/MS on a Q Exactive mass
301 spectrometer (Thermo Scientific) coupled to an EASY-nLC 1000 liquid chromatography
302 system via an EASY-Spray ion source (Thermo Scientific) with a 75 $\mu\text{m} \times 500$ mm
303 EASY-Spray column (Thermo Scientific) heated to 40 °C. An elution gradient duration of
304 240 min was used, fractionating mostly over the 3-40% acetonitrile range. Data were
305 acquired in the data-dependent acquisition mode. Full scan spectra (300-1800 Th) were
306 acquired with resolution of 70,000 at 400 Th (after accumulation to a target value of
307 1,000,000 with maximum injection time of 20 ms). The ten most intense ions were
308 fragmented by higher-energy collisional dissociation (HCD) and measured with
309 resolution 17,500 at 200 m/z and a target value of 500,000, with a maximum injection
310 time of 60 ms. Intensity threshold was 2.1×10^4 . Unassigned, +1 and >8+ charge peptides
311 were excluded, and peptide matching was set to “preferred”. A 40 second dynamic
312 exclusion list was applied.

313 For TMT-label MS analysis samples were processed as previously described (23).
314 Two μg of each sample were analyzed on an Orbitrap Fusion Lumos mass
315 spectrometer coupled to a Proxeon EASY-nLC 1200 liquid chromatography pump (both
316 Thermo Fisher Scientific) and a $100\ \mu\text{m} \times 35\ \text{cm}$ microcapillary column packed with
317 Accucore C18 resin ($2.6\ \mu\text{m}$, $150\ \text{\AA}$; Thermo Fisher). Peptides were fractionated over a
318 150 min gradient of 3 – 25% acetonitrile in 0.125% formic acid. An MS³-based TMT
319 method was used, as described previously (24).

320

321 Raw MS data analysis

322 Raw MS data files were processed using MaxQuant (25, version 1.5.8.3) using default
323 settings. MS/MS spectra were searched against the UniProt human proteome sequence
324 database. The MaxLFQ algorithm was implemented, applying a minimum ratio count of
325 2. For label-free samples the ‘match between runs’ option with default settings was
326 enabled. TMT-labelled samples were quantified by reporter ion MS³ – TMT10plex (Lys
327 & N-terminal 126C-130N), with a reporter mass tolerance of 0.003 Da. One percent
328 FDR filtering was applied at protein and peptide levels.

329

330 MS data processing

331 Further MS data analysis was performed using Perseus (26, version 1.5.8.5). ‘Reverse’
332 proteins, proteins ‘only identified by site’, and all non-human contaminants and human
333 contaminants, except cytoskeletal components, were filtered out. Data were log₂
334 transformed. The filtered APC AE-MS data set contained 5,571 identified proteins, of
335 which 5,521 were measured. From these only proteins measured in all four replicates of

336 at least one IP with N-APC, C-APC or control antibody were carried forward (4,016
337 proteins). Missing values were imputed from a normal distribution using standard
338 settings (width: $0.3 \times$ standard deviation of measured values, down shift: 1.8 in units of
339 standard deviation of measured values).

340 The filtered label-free proteome data set contained 5,982 identified proteins, of which
341 4,927 were measured in at least three replicates of at least one condition and only these
342 were used for further analysis. Missing values were imputed from a normal distribution.

343 The filtered TMT proteome data set contained 6,949 identified proteins, of which 6,923
344 were measured in all analyzed samples. Only these proteins were used for further
345 analysis.

346 Enrichment analysis of category terms within the group of potential APC interactors
347 identified by AE-MS (171 proteins) relative to all proteins measured in this experiment
348 (4,016 proteins) was calculated by Fisher Exact Test using default settings with a
349 Benjamini-Hochberg FDR <0.02 used for truncation.

350

351 Network generation

352 The APC interaction network was generated in Cytoscape (27, version 3.5.0) using
353 information on APC interactors listed in the IntAct Molecular Interaction Database
354 and/or BioGRID interaction repository. Low-confidence links (IntAct MI score <0.6),
355 individual nodes detached from the network, and indirect APC interactors with less than
356 two connections were deleted. The network layout was generated using the Weak
357 Clustering algorithm and the IntAct MI score for edge weighting within the Cytoscape
358 Allegro Layout App.

359

360

361 **Results**

362 Identification of APC-interacting proteins by affinity enrichment-mass spectrometry (AE- 363 MS)

364 For our initial discovery experiments, we used HeLa cells, which express relatively high
365 amounts of wild-type APC that can be efficiently depleted by siRNA. This allowed us to
366 measure protein binding to, and regulation by, APC in the same cell line. APC-
367 containing protein complexes were co-immunoprecipitated using two APC-specific
368 monoclonal antibodies that recognize N- and C-terminal domains, respectively. An
369 isotype-matched antibody against the viral V5 peptide was used as control. Co-
370 immunoprecipitation (Co-IP) with each antibody was performed in quadruplicate.
371 Samples were analyzed by label-free tandem mass spectrometry (LC-MS/MS). We only
372 considered the 4,016 proteins that were detected in all four replicates of Co-IP's with
373 either antibody for further analysis. Pearson correlation coefficients >0.9 for label-free
374 quantification (LFQ) intensities measured across replicates and a clear separation of N-
375 APC, C-APC and control Co-IPs by principal component analysis (PCA) indicated good
376 experimental reproducibility (Supplementary Figures S1A and B). Significant enrichment
377 of proteins in APC-specific versus control Co-IPs was determined by considering both
378 permutation-based FDR (<0.01) and LFQ intensity fold-change (Supplementary Figure
379 S1C).

380 In total, 171 proteins were significantly enriched in APC-specific Co-IPs (Figure
381 1B and Supplementary Table S1). These proteins will be referred to hereafter as the

382 'APC interactome'. Eighty and 71 proteins were exclusively enriched in either C-APC or
383 N-APC Co-IPs, respectively. Antibody binding to APC is likely affected by protein
384 interactions at domains close to or overlapping with the antibody epitopes. This could
385 explain co-immunoprecipitation of distinct interactors with different APC-specific
386 antibodies. Consistently, C-APC and N-APC antibodies immunoprecipitated
387 overlapping, but distinct, pools of APC that may contain different subsets of binding
388 partners (Supplementary Figure S1D). Twenty proteins, including APC itself, were
389 significantly enriched in both APC Co-IPs and only half of these were previously
390 described APC interactors (28,29; Supplementary Table S1).

391 To rule out a HeLa cell-specific enrichment of proteins in APC Co-IPs, we
392 validated our AE-MS results in the human colon carcinoma cell line HCT116-Ha β 92,
393 which are homozygous for wild-type APC and hemizygous for wild-type β -catenin (30).
394 Thirteen of the novel APC-interacting proteins were selected to cover the range of
395 biological functions represented in the data set and based on antibody availability.
396 Consistent with results obtained by AE-MS, 12/13 proteins were enriched in APC Co-
397 IPs in both cell lines (Supplementary Figure S2).

398

399 The APC interactome is enriched for epithelial-specific GO cellular component terms

400 To identify underlying functional patterns, we analyzed the enrichment of gene ontology
401 (GO), protein family (Pfam), and Kyoto encyclopedia of genes and genomes (KEGG)
402 terms in the APC interactome. Thirty-one terms were significantly over-represented
403 (Benjamini-Hochberg FDR <0.02); the majority can be broadly categorized into three
404 cellular processes: (actin) cytoskeleton organization, cell-cell contact establishment, and

405 RNA processing (Figure 1C, Supplementary Table S1). APC-interacting proteins
406 associated with cytoskeletal organization included known and newly identified
407 interactors, including several SCAR complex components. The enrichment of terms
408 linked to RNA processing is consistent with APC's role as an RNA-binding protein (31).
409 Strikingly, many of the enriched terms are associated with cell-cell contacts and
410 constitute components characteristic of epithelial cells, e.g. "lateral plasma membrane",
411 "tight junctions", and "cell-cell adherens junction".

412

413 Generation of an integrated APC interaction network

414 To understand the relationship between interaction partners, we tested how our
415 interactome integrated into a network of previously identified APC-binding proteins. Our
416 interactome data set overlaid well with, and added substantially to, the network of
417 known APC-binding proteins (Figure 2). The integrated network revealed many direct
418 and indirect high-confidence links between newly identified and known APC interactors
419 suggesting potential APC-interacting protein complexes. In addition to the 'β-catenin
420 destruction complex' cluster, several sub-networks emerged from this analysis. Two of
421 these included proteins associated with 'LSM protein family' and 'SCAR complex',
422 respectively, and both categories were enriched in our APC interactome data set
423 (Figure 1C).

424 To validate our network analysis, we generated a control network using 171
425 proteins randomly selected from the APC AE-MS data set. Compared to the random
426 selection, our interactome exhibited superior integration into the network of known APC-
427 binding partners (Supplementary Figure S3).

428

429 APC affects the abundance of many proteins independently of β -catenin

430 Because our APC interactome included many binding partners that appeared unrelated
431 to Wnt signaling components, we aimed to determine whether APC is involved in the
432 regulation of proteins other than β -catenin, and independently of β -catenin-mediated
433 cellular effects. To this end, we depleted APC alone or together with β -catenin from
434 HeLa cells using siRNA and measured changes in protein abundance by mass
435 spectrometry (MS). Cells were harvested 72 hours after transfection and efficient
436 knockdown was confirmed by western blotting (WB, Supplementary Figure S4A).
437 Simultaneous knockdown of APC and β -catenin abrogated β -catenin target gene
438 activation, as verified by the inhibition of *AXIN2* mRNA transcription (Supplementary
439 Figure S4D). For each siRNA combination, we analyzed four and two experimental
440 replicates by label-free and TMT MS, respectively. Downstream analysis was applied to
441 6,923 proteins measured in all eight samples by TMT MS and 4,927 proteins measured
442 in at least three replicates of at least one condition by label-free MS. Reproducibility
443 between replicates was very good, as indicated by Pearson correlation coefficients
444 >0.97 and a clear separation of distinct siRNA treatments by PCA (Supplementary
445 Figure S4B and C).

446 To identify proteins that changed in abundance in response to APC depletion, but
447 independently of β -catenin, we compared TMT/LFQ intensities across conditions of all
448 measured proteins to an “ideal” intensity profile of a hypothetical β -catenin-independent
449 APC target. A negative APC target was defined as a protein that increased in
450 abundance in response to APC loss, independently of whether APC was depleted alone

451 or together with β -catenin, but which protein levels did not change in β -catenin siRNA
452 compared to control siRNA-treated cells (the intensity profile of an “ideal” negative APC
453 target is indicated in red in Figure 3A top right). Conversely, a positive APC target was
454 defined as a protein that decreased in abundance in response to APC depletion,
455 independent of β -catenin status. The 200 proteins with profiles most similar to the ideal
456 negative and positive APC target were selected based on Pearson correlation.
457 Significant β -catenin-independent APC targets were determined by applying an
458 additional cut-off of >1.5 fold-change in APC and APC+ β -catenin siRNA-treated
459 samples relative to control with a q -value <0.05 (TMT)/ 0.1 (LFQ). By TMT MS we
460 identified 53 and 85 proteins that significantly increased and decreased, respectively, in
461 response to APC depletion in a β -catenin-independent manner; by LFQ MS 11 proteins
462 increased and 11 decreased (Figure 3A/B and E/G). Four negatively and seven
463 positively regulated proteins were common to both data sets. This group of proteins was
464 not enriched in distinct GO terms (data not shown), but spanned a range of cellular
465 functions including apoptosis, ion transport, actin organization, and proliferation.

466 To compare APC’s β -catenin-dependent and -independent effects on protein
467 expression, we also identified proteins that changed in abundance in response to APC
468 depletion in a β -catenin-dependent manner. The number of these proteins was similar
469 to those regulated independently of β -catenin: 64 and 37 were negatively regulated, 86
470 and 103 were positively regulated when detected by TMT and LFQ MS respectively
471 (Figure 3C/D and F/H, Supplementary Table S2).

472

473 Some β -catenin-independent APC targets are also deregulated in human cancer

474 To determine if any of the identified β -catenin-independent APC targets are implicated
475 in colorectal cancer, we compared our results with a dataset describing proteomic
476 changes in human colorectal adenoma and adenocarcinoma compared to healthy
477 mucosa (32). Nineteen proteins present in our APC target list were also found to be
478 dysregulated – in the same direction – in human adenomas and/or carcinomas (Table
479 1). These results highlight that mis-expression of some proteins in colorectal cancer
480 could be a direct consequence of loss of WT APC rather than deregulated Wnt
481 signaling.

482

483 MINK1 interacts with full length and truncated APC

484 From the group of β -catenin-independent APC targets identified by total proteomics
485 analysis, six were also found to interact with APC. Amongst these, MINK1 stood out as
486 a potentially druggable serine/threonine kinase. We validated the interaction between
487 MINK1 and full-length APC by Co-IP and WB in two cell lines (Figure 4A). In agreement
488 with results obtained by MS, MINK1 was only enriched in Co-IPs with the N-APC
489 antibody (Supplementary Figure S5A). To rule out N-APC antibody cross-reactivity, we
490 repeated the experiment with lysate from APC-depleted cells. Confirming its specific
491 enrichment in APC protein complexes, the amount of co-immunoprecipitated MINK1
492 correlated with the levels of APC present in IP lysates (Supplementary Figure S5B).
493 Conversely, APC was also enriched in Co-IPs of over-expressed GFP-tagged MINK1
494 compared to GFP alone (Supplementary Figure S5C). We next tested whether MINK1
495 could also interact with truncated APC expressed in colorectal cancer cells. MINK1 co-

496 immunoprecipitated with APC fragments in both SW480 and Colo320 cells (Figure 4B).
497 The ~90 kDa N-terminal APC fragment expressed in Colo320 cells retains the armadillo
498 and oligomerization domain, but lacks all β -catenin and Axin binding sites and other C-
499 terminal domains. The ~220 kDa APC fragment expressed in SW480 cells includes the
500 four most N-terminal β -catenin binding sites. These data suggest that the interaction
501 between the two proteins is mediated by domains in the N-terminal third of APC.

502

503 MINK1 is negatively regulated by APC independently of β -catenin

504 Consistent with our proteomics data, MINK1 levels measured by WB significantly
505 increased after 72 h of APC depletion in HeLa and U2OS cells and this accumulation
506 was independent of changes in β -catenin (Figure 4C and Supplementary Figure S5D
507 and S6A). Similar to results obtained with the siRNA pool, transfection with either of the
508 individual APC siRNAs efficiently decreased APC levels and produced a concomitant
509 increase in MINK1 protein (Supplementary Figure S5E). We validated the effect of APC
510 loss on MINK1 levels *in vivo* by measuring protein expression in intestinal tissue from
511 *Apc* mutant and wild-type mice. Mink1 protein was increased by 2.3-fold (± 0.4 SD) in
512 *Apc*^{Min/+} versus control animals (Figure 5A and 5B). In addition, we addressed whether
513 this regulatory relationship is conserved across species. We generated mosaic follicular
514 epithelia in *Drosophila melanogaster* egg chambers carrying clones of
515 double *APC1*, *APC2* mutant cells (marked by loss of NLS::RFP expression). Measuring
516 levels of a YFP-fused Misshapen protein – the closest orthologue in *Drosophila* -
517 (Msn::YFP) using live microscopy revealed that Msn::YFP levels were significantly
518 higher in cells that did not express APC1 and APC2 (Figure 5C-F).

519

520 Parallels between the regulation of MINK1 and β -catenin protein abundance

521 We hypothesized that APC regulates the abundance of MINK1 – similarly to β -catenin –
522 post-transcriptionally. Transfection with APC siRNA resulted in a significant up-
523 regulation of *AXIN2* mRNA, and this increase was efficiently inhibited when APC and β -
524 catenin were depleted simultaneously. In contrast, *MINK1* mRNA increased moderately
525 but changes in *MINK1* mRNA did not correlate with changes in MINK1 protein
526 abundance (Figure 6A and 4C).

527 We further tested whether the degradation of MINK1, similarly to β -catenin, was
528 dependent on the action of an E3 ubiquitin ligase. Treatment with the NEDD8-activating
529 enzyme selective inhibitor MLN4924, which inhibits cullin-RING ubiquitin ligase activity
530 (33), reproducibly induced a two-fold increase in MINK1 after 24 h (Figure 6B and
531 Supplementary Figure S6B).

532

533 MINK1 localizes to cell-cell junctions and enhances cell adhesion and proliferation

534 To address how elevated MINK1 could contribute to cellular processes affected by *APC*
535 mutations, we determined its sub-cellular localization. In agreement with a previous
536 study (34), immunofluorescence staining showed an enrichment of signal in the
537 perinuclear region (Supplementary Figure S6C). Nevertheless, a similar signal was
538 present in MINK1 knockout cells, suggesting cross-reactivity of this MINK1 antibody
539 with Golgi components. Indeed, the MINK1 antibody used for immunofluorescence
540 recognized additional proteins by WB (Supplementary Figure S6D, the MINK1 antibody
541 we used for WB was unsuitable for immunofluorescence).

542 To overcome this problem, we generated cells expressing endogenously
543 mNeonGreen-tagged MINK1, enabling us to study its localization live in un-fixed cells
544 (Supplementary Figure S6D). Although fluorescence intensity was low, mNeonGreen
545 signal was clearly enriched at tips of protrusions (*) and at lateral plasma membranes
546 (arrow heads) in areas of cell-cell contact (Figure 6C). No signal enrichment was
547 detected in 'free' regions of the plasma membrane without adjoining cells. Consistent
548 with a role for MINK1 in adhesion, overexpression of MINK1 resulted in a significant
549 increase in cell attachment to collagen (Figure 6D and Supplementary Figure S6E).
550 Furthermore, proliferation of colorectal cancer cells in which regulation of MINK1 by
551 APC was lost (Supplementary Figure S6F), was significantly reduced when MINK1 was
552 depleted using siRNA (Figure 6E).

553

554

555 **Discussion**

556 We aimed to elucidate – on a global scale – the diverse molecular roles of APC, with an
557 emphasis on its functions beyond the β -catenin destruction complex. To this end, we
558 applied an untargeted approach using label-free and TMT-based MS to assemble an
559 APC interactome and, furthermore, to identify the β -catenin-independent APC-regulated
560 proteome. These data sets provide a useful resource for the identification of proteins
561 that participate in and coordinate Wnt-independent functions of APC.

562 In contrast to previous interaction studies, we used endogenous, full-length, and
563 non-tagged APC in our AE-MS experiment. The identification of additional PDZ domain-
564 containing APC interaction partners highlighted the benefit of this approach.

565 Strikingly, the APC interactome was highly enriched for proteins that are part of cellular
566 components characteristic for epithelial cells, as well as members of the membrane
567 associated “guanylate kinase” (MAGUK) protein family, and PDZ-domain containing
568 proteins (Figure 1C). MAGUK proteins are implicated in the establishment of epithelial
569 cell polarity (35). Furthermore, the function of APC in epithelia is – at least partly –
570 mediated by PDZ domain-containing proteins (36). In addition, STRIPAK complex
571 components formed a highly connected cluster within the APC interaction network
572 (Figure 2). APC and the STRIPAK component Striatin localize interdependently to cell-
573 cell junctions in epithelial cells and depletion of Striatin and APC affects tight junction
574 organization (8). It is conceivable that binding to APC regulates the sub-cellular
575 localization, activity, and/or expression of these epithelial-characteristic proteins, in turn
576 controlling cellular adhesion and establishment of epithelial polarity. Investigating these
577 interactions further will provide useful insights into the mechanisms that regulate APC
578 function in different tissues and further improve our understanding of the phenotypes
579 associated with APC loss. Such studies could reveal why *APC* germ line mutations in
580 FAP patients result in cancerous lesions of the gut epithelium, while other organs often
581 remain unaffected.

582 Measuring proteome-wide effects of APC loss revealed a set of β -catenin-
583 independent APC targets, supporting a role of APC in the regulation of protein
584 abundance beyond the β -catenin destruction complex (Figure 3). Similar to the effect on
585 β -catenin, depletion of APC resulted in the accumulation of some proteins, while the
586 levels of others were negatively affected, suggesting that APC can also inhibit
587 degradation of some of its targets. Strikingly, the number of proteins regulated by APC

588 independent and dependent of β -catenin was very similar. It is important to
589 acknowledge that untargeted MS is biased towards detection of more abundant
590 proteins. Consistently, many established, but low-abundant, β -catenin targets, such as
591 Myc and Axin2, were not detected and are thus absent from our analysis. However, this
592 bias operates in both sets of targets equally. Changes in the abundance of individual
593 APC targets could result from alterations in PTMs and/or protein stability – as is the
594 case for β -catenin. This is supported by previous findings in *Drosophila*, where loss of
595 APC2 causes proteome-wide and β -catenin-independent changes in post-translational
596 modifications that also affect protein stability of some proteins (37). In addition, effects
597 on transcription may also contribute to the differences in protein abundance observed in
598 our study.

599 Since we have used HeLa cells (which we chose for technical reasons, see
600 Results section) in our discovery MS experiments, we were unable to identify potential
601 APC interacting proteins and/or targets which expression is e.g. restricted to intestinal
602 epithelial cells. This limitation will need to be addressed in future studies - ideally using
603 human/mouse intestinal tissue expressing wild-type and mutant APC.

604 At present, it remains unclear how changes in these APC targets contribute to
605 the functional consequences of APC loss observed *in vivo*. As a first step towards
606 addressing this question, we compared our data set with data describing proteome-wide
607 changes in colon adenomas and carcinomas (32). Several of the β -catenin-independent
608 APC targets we identified were also found to be dysregulated in colorectal adenomas
609 and/or tumors (Table 1). Among these, NDRG1, which was downregulated in APC-
610 depleted cells in our study and also in cancerous tissue, might be of particular interest.

611 NDRG1 has been established as a tumor suppressor in colorectal cancer cells based
612 on its negative effects on metastasis and apoptosis (38).

613 Collectively, our results suggest that part of the protein expression changes
614 observed in colorectal cancer are independent of increased Wnt target gene
615 expression. Investigating the functional impact of these changes will further help to
616 elucidate how APC loss contributes to cancer development beyond de-regulated β -
617 catenin. Accounting for these effects will be especially important when considering
618 cancer therapy, as they reveal that consequences of mutant APC protein cannot be fully
619 rectified by restoring normal Wnt signaling.

620

621 Little is known about the functions of MINK1 or the regulation of its activity and/or its
622 abundance. Existing data implicate MINK1 in cell adhesion, cell migration and planar
623 cell polarity (PCP; 34,39,40) - processes crucial for epithelial biology. Furthermore,
624 MINK1 kinase activity is required for completion of cytokinesis (41). Importantly, these
625 processes are also deregulated in APC mutant tissues (42-44). Moreover, TRAF2 and
626 NCK-interacting protein kinase (TNIK), which shares high sequence homology with
627 MINK1, is emerging as a promising target for colorectal cancer therapy, as it regulates
628 the activity of the TCF-4/ β -catenin transcription complex (45).

629 Collectively, our results indicate that MINK1 is regulated by APC in a manner
630 similar to β -catenin (Figure 4 and 6). Importantly, increased Mink1/Msn levels after loss
631 of wild-type Apc/APC1,2 were also observed *in vivo*, in mouse intestinal tissue and
632 follicular cells in *Drosophila* (Figure 5). Consistent with its localization to cell-cell
633 junctions, over-expression of MINK1-GFP resulted in increased cell adhesion (Figure

634 6C, D). This is in contrast to a previous study, in which cells overexpressing full-length
635 MINK1 did not grow in clusters but in isolation, suggesting decreased adhesion between
636 cells (34). However, in this case, the effects were not quantified and additional studies
637 of MINK1 overexpression on cell-cell adhesion do not exist. It is conceivable, that
638 enhanced cell adhesion due to elevated MINK1 expression contributes to the reduced
639 cell migration observed in *APC* mutant tissue (43, 46). Moreover, directionality of cell
640 migration could be disturbed when MINK1 expression is deregulated in response to
641 *APC* loss. Evidence for a role of mammalian MINK1 in PCP is limited (39); however, a
642 role for its *Drosophila* homologue *Msn* in epithelial PCP has been firmly established
643 (47). In flies, both *Apc* and *Msn* act downstream of Dishevelled, which was described as
644 a 'branchpoint' between the canonical Wnt and the non-canonical PCP pathway (48).
645 Our results indicate that regulation of *Msn* by *APC* is conserved in flies (Figure 5C-F),
646 suggesting an additional level of crosstalk between these signaling pathways.
647 Furthermore, knockdown of MINK1 in colorectal cancer cells resulted in a significant
648 reduction in proliferation, comparable to the effect seen with β -catenin depletion (Figure
649 6E). Future experiments will focus on elucidating the molecular mechanisms of MINK1
650 regulation by *APC* and the identification of downstream effectors mediating the effects
651 of MINK1 overexpression on cell adhesion.

652

653

654 **Acknowledgments**

655 We would like to acknowledge the Nikon Imaging Center at Harvard Medical School and
656 the Dundee Tissue Imaging Facility at the School of Life Sciences, University of Dundee

657 (supported by Wellcome grant WT101468) for providing help and equipment for
658 microscopy imaging of cells and live *Drosophila* samples, respectively. Stocks from the
659 Bloomington *Drosophila* Stock Center, which is supported by NIH grant P40OD018537,
660 were used in this study. We would like to thank C. MacKintosh, G. Murugesan, R. Hay,
661 E. Jaffrey, T. Kurz, and M. Keuss (all University of Dundee) for sharing advice and
662 reagents. For their help in the realization of TMT MS experiments we would like to thank
663 S. Gygi and the Taplin Mass Spectrometry Facility at Harvard Medical School.

664

665

666 **References**

- 667 1. Miyoshi, Y., Nagase H., Ando H., Horii A., Ichii S., Nakatsuru S., Aoki T., Miki Y.,
668 Mori T., and Nakamura Y. (1992). Somatic mutations of the *APC* gene in
669 colorectal tumors: mutation cluster region in the *APC* gene. *Hum. Mol. Genet.* *1*,
670 229–233.
- 671 2. Powell, S.M., Zilz, N., Beazer-Barclay, Y., Bryan, T.M., Hamilton, S.R.,
672 Thibodeau, S.N., Vogelstein, B., and Kinzler, K.W. (1992). *APC* mutations occur
673 early during colorectal tumorigenesis. *Nature* *359*, 235–237.
- 674 3. Leoz, M.L., Carballal, S., Moreira, L., Ocaña, T., and Balaguer, F. (2015). The
675 genetic basis of familial adenomatous polyposis and its implications for clinical
676 practice and risk management. *Appl. Clin. Genet.* *8*, 95–107.
- 677 4. Stamos, J.L., and Weis, W.I. (2013). The β -catenin destruction complex. *Cold*
678 *Spring Harb. Perspect. Biol.* *5*, a007898.
- 679 5. Polakis, P. (2000). Wnt signaling and cancer. *Genes Dev.* *14*, 1837–1851.

- 680 6. Cheung, A.F., Carter, A.M., Kostova, K.K., Woodruff, J.F, Crowley, D., Bronson,
681 R.T., Haigis, K.M., Jacks, T. (2010). Complete deletion of *Apc* results in severe
682 polyposis in mice. *Oncogene* 29, 1857-1864.
- 683 7. Nelson, S., Näthke, I.S. (2013). Interactions and functions of the Adenomatous
684 polyposis coli (APC) protein at a glance. *J. Cell Sci.* 126, 873-877.
- 685 8. Breitman, M., Zilberberg, A., Caspi, M., and Rosin-Arbesfeld, R. (2008). The
686 armadillo repeat domain of the APC tumor suppressor protein interacts with
687 Striatin family members. *Biochim. Biophys. Acta* 1783, 1792–1802.
- 688 9. Bandyopadhyay, S., Chiang, C., Srivastava, J., Gersten, M., White, S., Bell, R.,
689 Kurschner, C., Martin, C.H., Smoot, M., Sahasrabudhe, S., et al. (2010). A
690 human MAP kinase interactome. *Nature Methods* 7, 801-805.
- 691 10. Hein, M.Y., Hubner, N.C., Poser, I., Cox, J., Nagaraj, N., Toyoda, Y., Gak, I.A.,
692 Weisswange, I., Mansfeld, J., Buchholz, F., et al. (2015). A human interactome in
693 three quantitative dimensions organized by stoichiometries and abundances. *Cell*
694 163, 712–723.
- 695 11. Song, J., Hao, Y., Du, Z., Wang, Z., and Ewing, R.M. (2012). Identifying novel
696 protein complexes in cancer cells using epitope-tagging of endogenous human
697 genes and affinity-purification mass spectrometry. *J. Proteome Res.* 11, 5630–
698 5641.
- 699 12. Harris, B.Z., and Lim, W.A. (2001). Mechanism and role of PDZ domains in
700 signaling complex assembly. *J. Cell Sci.* 114, 3219–3231.

- 701 13. Joslyn, G., Richardson, D.S., White, R., and Alber, T. (1993). Dimer formation by
702 an N-terminal coiled coil in the APC protein. *Proc. Natl. Acad. Sci. USA* 90,
703 11109–11113.
- 704 14. Kim, N.G., Xu, C., Gumbiner, B.M. (2009). Identification of targets of the Wnt
705 pathway destruction complex in addition to beta-catenin. *Proc. Natl. Acad. Sci. U*
706 *S A* 106, 5165-5170.
- 707 15. Coyaud, E., Mis, M., Laurent, E.M.N., Dunham, W.H., Couzens, A.L., Robitaille,
708 M., Gingras, A.C., Angers, S., Raught, B. (2015). BiOID-based identification of
709 Skp Cullin F-box (SCF) β -TrCP1/2 E3 ligase substrates. *Mol. Cell. Proteomics* 14,
710 1781-1795.
- 711 16. Rojas-Fernandez, A., Herhaus, L., Macartney, T., Lachaud, C., Hay, R.T.,
712 Sapkota, G.P. (2015). Rapid generation of endogenously driven transcriptional
713 reporters in cells through CRISPR/Cas9. *Sci. Rep.* 5, 9811.
- 714 17. Aberle, H., Bauer, A., Stappert, J., Kispert, A., Kemler, R. (1997). Beta-catenin is
715 a target for the ubiquitin-proteasome pathway. *EMBO J.* 16, 3797-3804.
- 716 18. Midgley, C.A., White, S., Howitt, R., Save, V., Dunlop, M.G., Hall, P.A., Lane,
717 D.P., Wyllie, A.H., and Bubb, V.J. (1997). APC expression in normal human
718 tissues. *J. Pathol.* 181, 426-433.
- 719 19. Hinck, L., Näthke, I.S., Papkoff, J., Nelson, W.J. (1994). Dynamics of
720 cadherin/catenin complex formation: novel protein interactions and pathways of
721 complex assembly. *J. Cell Biol.* 125, 1327-1340.

- 722 20. Schindelin, J., Arganda-Carreras, I., Frise, E., Kaynig, V., Longair, M., Pietzsch,
723 T., Preibisch, S., Rueden, C., Saalfeld, S., Schmid, B., et al. (2012). Fiji: an open-
724 source platform for biological-image analysis. *Nat. Methods* 9, 676-682.
- 725 21. Pfaffl, M.W. (2001). A new mathematical model for relative quantification in real-
726 time RT-PCR. *Nucleic Acids Res.* 29, e45.
- 727 22. Shevchenko, A., Tomas, H., Havlis, J., Olsen, J.V., and Mann, M. (2006). In-gel
728 digestion for mass spectrometric characterization of proteins and proteomes.
729 *Nat. Protoc.* 1, 2856-2860.
- 730 23. Paulo, J.A., O'Connell, J.D., Everley, R.A., O'Brian, J., Gygi, M.A., and Gygi, S.P.
731 (2016). Quantitative mass spectrometry-based multiplexing compares the
732 abundance of 5000 *S. cerevisiae* proteins across 10 carbon sources. *J.*
733 *Proteomics* 148, 85-93.
- 734 24. Paulo, J.P., O'Connell, J.D., and Gygi, S.P. (2016). A Triple Knockout (TKO)
735 proteomics standard for diagnosing ion interference in isobaric labeling
736 experiments. *J. Am. Soc. Mass. Spectrom.* 27, 1620-1625.
- 737 25. Cox, J., and Mann, M. (2008). MaxQuant enables high peptide identification
738 rates, individualized p.p.b.-range mass accuracies and proteome-wide protein
739 quantification. *Nat. Biotechnol.* 26, 1367-1372.
- 740 26. Tyanova, S., Temu, T., Sinitcyn, P., Carlson, A., Hein, M.Y., Geiger, T., Mann,
741 M., and Cox, J. (2016). The Perseus computational platform for comprehensive
742 analysis of (prote)omics data. *Nat. Methods* 13, 731-740.
- 743 27. Shannon, P., Markiel, A., Ozier, O., Baliga, N.S., Wang, J.T., Ramage, D., Amin,
744 N., Schwikowski, B., and Ideker, T. (2003). Cytoscape: a software environment

745 for integrated models of biomolecular interaction networks. *Genome Res.* *13*,
746 2498–2504.

747 28. Orchard, S., Ammari, M., Aranda, B., Breuza, L. Briganti, L., Broackes-Carter, F.,
748 Campbell, N.H., Chavali, G., Chen, C., del Toro, N., et al. (2014). The MIntAct
749 project–IntAct as a common curation platform for 11 molecular interaction
750 databases. *Nucleic Acids Res.* *42*, D358–D363.

751 29. Stark, C., Breitkreutz, B.-J., Reguly, T., Boucher, L., Breitkreutz, A., and Tyers,
752 M. (2006). BioGRID: a general repository for interaction datasets. *Nucleic Acids*
753 *Res.* *34*, D535–D539.

754 30. Kim, J.-S., Crooks, H., Dracheva, T., Nishanian, T.G., Singh, B., Jen, J., and
755 Waldman, T. (2002). Oncogenic β -catenin is required for bone morphogenetic
756 protein 4 expression in human cancer cells. *Cancer Res.* *62*, 2744–2748.

757 31. Preitner, N., Quan, J., Nowakowski, D.W., Hancock, M.L., Shi, J., Tcherkezian,
758 J., Young-Pearse, T.L., and Flanagan, J.G. (2014). APC is an RNA-binding
759 protein, and its interactome provides a link to neural development and
760 microtubule assembly. *Cell* *158*, 368–382.

761 32. Wiśniewski, J.R., Duś-Szachniewicz, K., Ostasiewicz, P., Ziółkowski, P., Rakus,
762 D., and Mann, M. (2015). Absolute proteome analysis of colorectal mucosa,
763 adenoma, and cancer reveals drastic changes in fatty acid metabolism and
764 plasma membrane transporters. *J. Proteome Res.* *14*, 4005–4018.

765 33. Soucy, T.A., Smith, P.G., Milhollen, M.A., Berger, A.J., Gavin, J.M., Adhikari, S.,
766 Brownell, J.E., Burke, K.E., Cardin, D.P., Critchley, S., et al. (2009). An inhibitor

767 of NEDD8-activating enzyme as a new approach to treat cancer. *Nature* 458,
768 732–736.

769 34. Hu, Y., Leo, C., Yu, S., Huang, B.C.B., Wang, H., Shen, M., Luo, Y., Daniel-
770 Issakani, S., Payan, D.G., and Xu, X. (2004). Identification and functional
771 characterization of a novel human misshapen/Nck interacting kinase-related
772 kinase, hMINK beta. *J. Biol. Chem.* 279, 54387–54397.

773 35. Caruana, G. (2002). Genetic studies define MAGUK proteins as regulators of
774 epithelial cell polarity. *Int. J. Dev. Biol.* 46, 511-518.

775 36. Mimori-Kiyosue, Y., Matsui, C., Sasaki, H., and Tsukita, S. (2007). Adenomatous
776 polyposis coli (APC) protein regulates epithelial cell migration and
777 morphogenesis via PDZ domain-based interactions with plasma membranes.
778 *Genes to Cells* 12, 219-233.

779 37. Blundon, M.A., Schlesinger, D.R., Parthasarathy, A., Smith, S.L., Kolev, H.M.,
780 Vinson, D.A., Kunttas-Tatli, E., McCartney, B.M., Minden, J.S. (2016). Proteomic
781 analysis reveals APC-dependent post-translational modifications and identifies
782 novel regulator of β -catenin. *Development* 143, 2629-2640.

783 38. Mi, L., Zhu, F., Yang, X., Lu, J., Zheng, Y., Zhao, Q., Wen, X., Lu, A., Wang, M.,
784 Zheng, M., et al. (2017). The metastatic suppressor NDRG1 inhibits EMT,
785 migration and invasion through interaction and promotion of caveolin-1
786 ubiquitylation in human colorectal cancer cells. *Oncogene* 36, 4323-4335.

787 39. Daulat, A.M., Luu, O., Sing, A., Zhang, L., Wrana, J.L., McNeill, H., Winklbauer,
788 R., and Angers, S. (2012). Mink1 regulates β -catenin-independent Wnt signaling
789 via Prickle phosphorylation. *Mol. Cell Biol.* 32, 173–185.

- 790 40. Mikrykov, A., and Moss, T. (2012). Agonistic and antagonistic roles for TNIK and
791 MINK in non-canonical and canonical Wnt signalling. *PLoS One* 7, e43330.
- 792 41. Hyodo, T., Ito, S., Hasegawa, H., Asano, E., Maeda, M., Urano, T., Takahashi,
793 M., Hamaguchi, M., and Senga, T. (2012). Misshapen-like kinase 1 (MINK1) is a
794 novel component of striatin-interacting phosphatase and kinase (STRIPAK) and
795 is required for the completion of cytokinesis. *J. Biol. Chem.* 287, 25019–25029.
- 796 42. Wong, M.H., Hermiston, M.L., Syder, A.J., and Gordon, J.I. (1996). Forced
797 expression of the tumor suppressor adenomatosis polyposis coli protein induces
798 disordered cell migration in the intestinal epithelium. *Proc. Natl. Acad. Sci. USA*
799 93, 9588–9593.
- 800 43. Mahmoud, N.N., Boolbol, S.K., Bilinski, R.T., Martucci, C., Chadburn, A., and
801 Bertagnolli, M.M. (1997). *Apc* gene mutation is associated with a dominant-
802 negative effect upon intestinal cell migration. *Cancer Res.* 57, 5045–5050.
- 803 44. Caldwell, C.M., Green, R.A., and Kaplan, K.B. (2007). APC mutations lead to
804 cytokinetic failures in vitro and tetraploid genotypes in *Min* mice. *J. Cell Biol.* 178,
805 1109-1120.
- 806 45. Yamada, T., and Masuda, M. (2017). Emergence of TNIK inhibitors in cancer
807 therapeutics. *Cancer Sci.* 108, 818-823.
- 808 46. Sansom, O.J., Reed, K.R., Hayes, A.J., Ireland, H., Brinkmann, H., Newton, I.P.,
809 Battle, W., Simon-Assmann, P., Clevers, H., Nathke, I.S., et al. (2004). Loss of
810 *Apc in vivo* immediately perturbs Wnt signaling, differentiation, and migration.
811 *Genes Dev.* 18, 1385-1390.

- 812 47. Paricio, N., Feiguin, F., Boutros, M., Eaton, S., and Mlodzik, M. (1999). The
813 *Drosophila* STE20-like kinase Misshapen is required downstream of the Frizzled
814 receptor in planar polarity signaling. *EMBO J.* 18, 4669-4678.
- 815 48. Wallingford, J.B., and Habas, R. (2005). The developmental biology of
816 Dishevelled: an enigmatic protein governing cell fate and cell polarity.
817 *Development* 132, 4421-4436.
- 818 49. Tusher, V.G., Tibshirani, R., and Chu, G. (2001). Significance analysis of
819 microarrays applied to the ionizing radiation response. *Proc. Natl. Acad. Sci.*
820 *USA* 98, 5116-5121.
- 821

822 **Tables**

823 Table 1. Overlap between β -catenin-independent APC targets identified in this study and proteins mis-expressed in
 824 colorectal polyps and/or tumors (31).

Protein name (identified by TMT and/or LFQ)	Log2 fold change			q value			Log2 fold change (Wiśniewski et al. 2015 – ref 31)	
	APC siRNA /control	β -catenin siRNA /control	APC+ β -catenin siRNA /control	APC siRNA /control	β -catenin siRNA /control	APC+ β -catenin siRNA /control	polyps /normal	tumor /normal
60S ribosomal export protein NMD3 (TMT/LFQ)	2.79/4.54	0.89/2.62	2.02/3.77	<0.001	0.019/0.027	<0.001	0.67	1.46
Peptidyl-prolyl cis-trans isomerase FKBP10 (TMT/LFQ)	1.16/1.13	0.49/0.74	1.00/1.03	0.004/0.04	0.062/0.238	0.003/0.087	0.06	1.95
Melanoma-associated antigen D2 (LFQ)	1.52	1.04	1.29	0.021	0.09	0.047	1.07	2.21
Nucleolar protein 58 (LFQ)	0.93	0.48	1.03	0.059	0.238	0.098	1.5	1.25
6-pyruvoyl tetrahydrobiopterin synthase (TMT)	1.97	0.51	1.29	<0.001	0.057	0.007	1.67	0.66
Glycerophosphocholine phosphodiesterase GPCPD1 (TMT)	1.46	0.41	0.94	0.012	0.083	0.007	1.34	1.19
Hermansky-Pudlak syndrome 5 protein (TMT)	0.74	0.28	0.67	0.002	0.154	0.011	1.14	0.68
Ubiquitin carboxyl-terminal hydrolase 8 (TMT)	1.04	0.44	0.73	0.003	0.069	0.006	0.58	-0.23
Zinc finger protein 622 (TMT)	1.26	-0.19	0.74	0.006	0.283	0.006	0.44	0.80
Ras-related protein Rab-14 (TMT/LFQ)	-1.77/ -1.48	-0.08/ -0.24	-1.39/ -1.01	<0.001/ 0.025	0.568/ 0.384	<0.001/ 0.086	-0.55	-0.27
Aldehyde dehydrogenase family 1 member A3 (LFQ)	-1.98	-0.58	-1.45	0.009	0.192	0.041	-1.14	-0.69
cAMP-dependent protein kinase type I-alpha regulatory subunit (TMT)	-0.71	0.09	-0.61	0.002	0.518	0.011	-0.77	-1.33

Dolichol-phosphate mannosyltransferase subunit 1 (TMT)	-1.09	-0.07	-0.93	0.004	0.617	0.008	-0.97	0.07
EH domain-containing protein 1 (TMT)	-0.60	-0.20	-0.60	0.006	0.229	0.014	-0.95	-0.78
Ferrochelatase, mitochondrial (TMT)	-1.17	-0.04	-0.71	0.005	0.751	0.011	-0.33	-1.54
Leucine zipper protein 1 (TMT)	-1.73	-0.20	-1.24	<0.001	0.267	0.006	0.85	-0.20
Moesin (TMT)	-1.15	-0.09	-0.79	0.003	0.543	0.006	-0.85	-1.06
Non-histone chromosomal protein HMG-14 (TMT)	-1.28	-0.20	-0.85	0.007	0.247	0.006	-0.81	-0.66
Protein NDRG1 (TMT)	-1.55	-0.41	-1.18	0.010	0.098	0.004	-0.17	-0.67

825

826 **Figure Legends**

827 Figure 1. Identification of APC-interacting and -regulated proteins.

828 **A** Experimental Outline. Proteins in APC-containing complexes and changes in protein
829 expression in response to siRNA-mediated depletion of APC and/or β -catenin were
830 analyzed by label-free and TMT-based mass spectrometry. The overlap between the
831 two data sets constitutes potential targets of alternative APC-containing complexes. **B**
832 Proteins significantly enriched in C- and/or N-APC Co-IPs. Log₂ fold change in mean
833 LFQ intensities between N-APC Co-IP vs. control IP (x-axis) plotted against log₂ fold
834 change in mean LFQ intensities between C-APC Co-IP vs. control IP (y-axis, n=4
835 experimental replicates). Significance determined by two-sided t-test with permutation-
836 based FDR <0.01 and $s_0 = 2$ used for truncation (49). **C** GO, Pfam and KEGG terms
837 significantly enriched in the APC interactome data set. Enrichment calculated by Fisher
838 Exact Test, significance determined by Benjamini-Hochberg corrected FDR <0.02.
839 Abbreviations: pos. - positive, reg. - regulation, comp.-med. - complex-mediated, nuc. -
840 nucleation, organiz. - organization.

841

842 Figure 2. APC interactome network.

843 Network integrating known (blue), newly identified (orange), and indirect (grey) APC
844 interaction partners. Nodes are labelled with corresponding gene names and node size
845 correlates with degree of connectivity, i.e. number of edges. Components of distinct
846 protein complexes (1, 3-5) and proteins associated with the cytoskeleton (2) cluster
847 together in sub-networks.

848

849 Figure 3. β -catenin-dependent and β -independent APC targets identified by TMT-label
850 MS (A-D) and label-free MS (E-H).

851

852 **A/E** Profiles of z-scored TMT (A) and LFQ (E) intensities of all measured proteins
853 across samples. Protein identified as negative and positive β -catenin-independent APC
854 targets are shown in orange and blue, respectively. Red lines show profiles for
855 hypothetical 'ideal' targets that increase/decrease in response to APC depletion, but
856 irrespective of a change in β -catenin. **B/G** Log₂ fold change in mean TMT (B) and LFQ
857 (G) intensities between APC siRNA and control siRNA treated samples (x-axis) plotted
858 against the log₂ fold change in mean intensities between β -catenin+APC siRNA and
859 control siRNA treated samples (y-axis). Proteins selected based on their intensity
860 profiles in **A/E** are shown in orange and blue, respectively. **C** and **D** Same as A, but for
861 β -catenin-dependent APC targets.

862 **A** Profiles of z-scored LFQ intensities of all measured proteins across samples. Protein
863 identified as negative and positive β -catenin-independent APC targets are shown in
864 orange and blue, respectively. Red lines show profiles for hypothetical 'ideal' targets
865 that increase/decrease in response to APC depletion, but irrespective of change in β -
866 catenin levels. **B** Log₂ fold change in mean LFQ intensities between APC siRNA and
867 control siRNA treated samples (x-axis) plotted against the log₂ fold change in mean
868 LFQ intensities between β -catenin+APC siRNA and control siRNA treated samples (y-
869 axis). Proteins selected based on their LFQ intensity profiles in **A** are shown in orange
870 and blue, respectively. **C** and **D** Same as A, but showing β -catenin-dependent APC
871 targets.

872

873 Figure 4. MINK1 binds to and is negatively regulated by APC.

874 **A** Co-IP of MINK1 with full-length, endogenous APC in HeLa and U2OS cells. **B** Co-IP
875 of MINK1 with C-terminally truncated APC in Colo320 and SW480 colorectal cancer
876 cells; both cell lines lack the second WT allele. **C** Changes in MINK1 proteins levels in
877 response to siRNA-mediated depletion of APC and/or β -catenin measured by WB.
878 Shown are means and SD relative to control samples from four independent
879 transfections. Significance relative to control determined by two-way ANOVA followed
880 by Dunnett's multiple comparison test; *: p value < 0.05, **: p value < 0.01.

881

882 Figure 5. Mink1/Msn levels increase in response to *Apc* loss *in vivo*.

883 **A** Expression of Mink1 in small intestinal tissue lysate from WT and *Apc*^{Min/+} mice
884 measured by WB, each lane represents lysate obtained from individual mice. The
885 *Apc*^{Min} fragment of approximately 90 kDa was present in mutant mice, but full-length
886 *Apc* (~310 kDa) was not detectable. **B** Quantification of WB shown in A. Shown is the
887 mean WB signal across the four mice per genotype relative to the signal in WT mice
888 and normalized to *Gapdh*. Significance relative to WT samples determined by un-
889 paired, two-tailed t test; p value: * < 0.05, ** < 0.01. **C** Live stage 8 *Drosophila* egg
890 expressing NLS::RFP and PH::RFP (magenta) under the control of a ubiquitous
891 promoter, and endogenous *Msn*::YFP (green). Two large *APC1*, *APC2* double mutant
892 clones within the follicular epithelium are identified by the absence of NLS::RFP and
893 delimited by arrowheads. **D** Magnification of one *APC1*, *APC2* double mutant clone
894 displayed in C. **E** Intensity profiles of RFP and *Msn*::YFP signal along the follicular

895 epithelium. **F** Msn signal intensity at the interface between *apc1⁻, apc2⁻ / apc1⁺,*
896 *apc2⁺* heterozygous cells (HT-ctrl, n=31), *apc1⁺, apc2⁺ / apc1⁺, apc2⁺* homozygous
897 control cells (HM-ctrl, n=31) and *apc1⁻, apc2⁻ / apc1⁻, apc2⁻* homozygous mutant cells
898 (HM-mut, n=38), normalized to the signal at heterozygous interfaces. In total ten clones
899 from then different egg chambers were analyzed. Significance determined by two-tailed
900 Mann-Whitney U test: p value: * = 0.0232, *** < 0.00001.

901

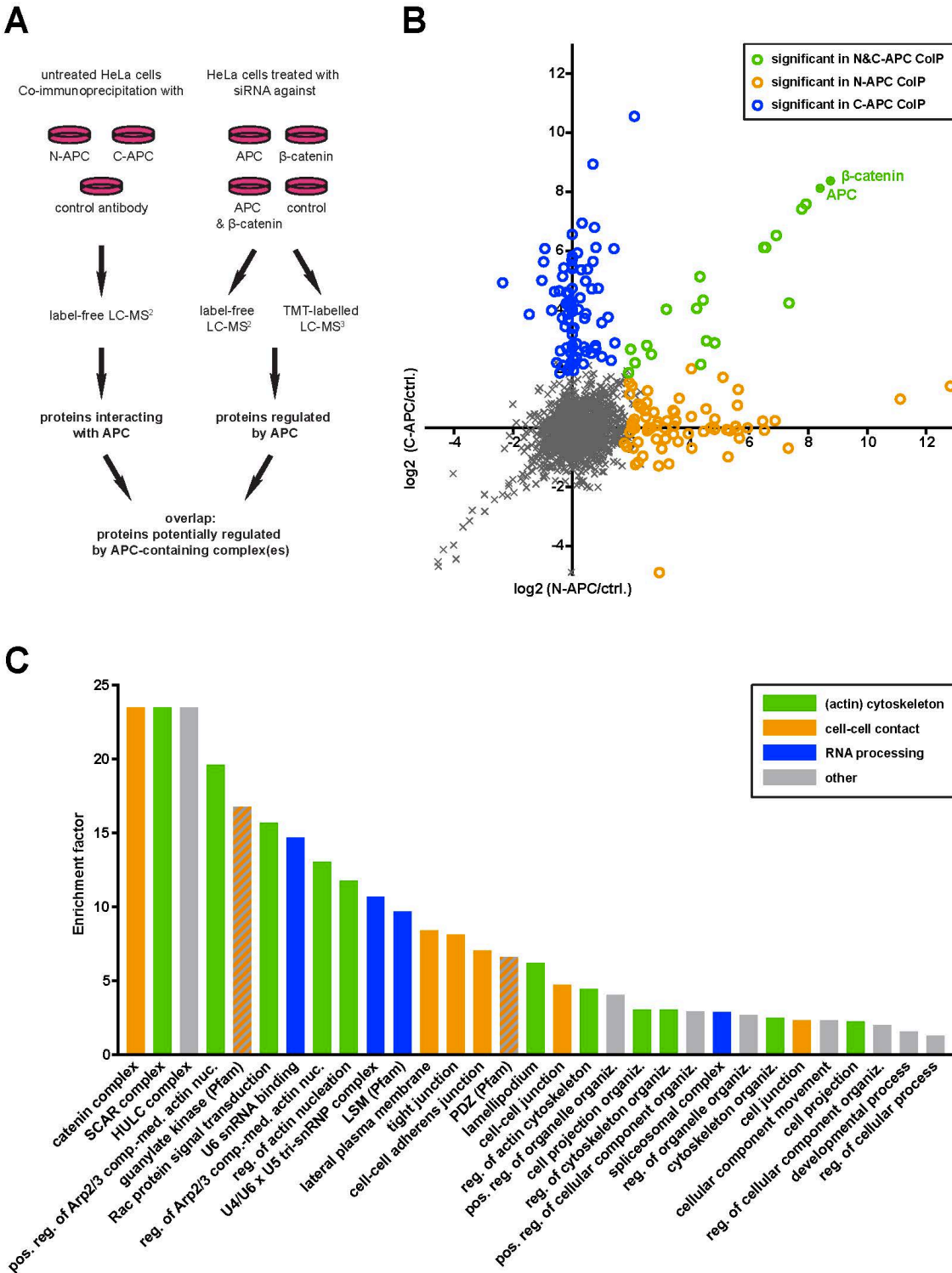
902 Figure 6. MINK1 localizes to cell-cell junctions and its overexpression enhances cell
903 adhesion.

904 **A** mRNA expression of *MINK1*, *CTNNB1*, and *AXIN2* measured by RT-qPCR 48 and 72
905 h after siRNA transfection. Indicated are mean expression levels relative to *ACTB*
906 expression with SD from four independent transfections. Significance determined by
907 one-way ANOVA followed by Dunnett's multiple comparison test; p value: * < 0.05, ** <
908 0.01, *** < 0.001. Note, the same HeLa *AXIN2* mRNA quantification data is also shown
909 in Supplementary Figure S4D. **B** MINK1 protein levels in HeLa cells after treatment with
910 neddylation inhibitor MLN4924 [3 μ M] as measured by WB. Shown are relative mean
911 signals normalized to DMSO-treated samples with SD from three independent
912 experiments. Significance determined by one-way ANOVA, **: p value < 0.01. **C** Live
913 imaging of HeLa SEC-C cells expressing endogenously mNeonGreen-tagged MINK1.
914 Scale bars: 10 μ m. **D** Adhesion assay with U2OS cells overexpressing MINK1-GFP and
915 GFP, respectively. Adhesion to collagen matrix after one hour was quantified by staining
916 of firmly attached cells with Crystal Violet. Indicated is mean absorbance with SD of
917 independent experiments with two different GFP/MINK1-GFP clones and eight technical

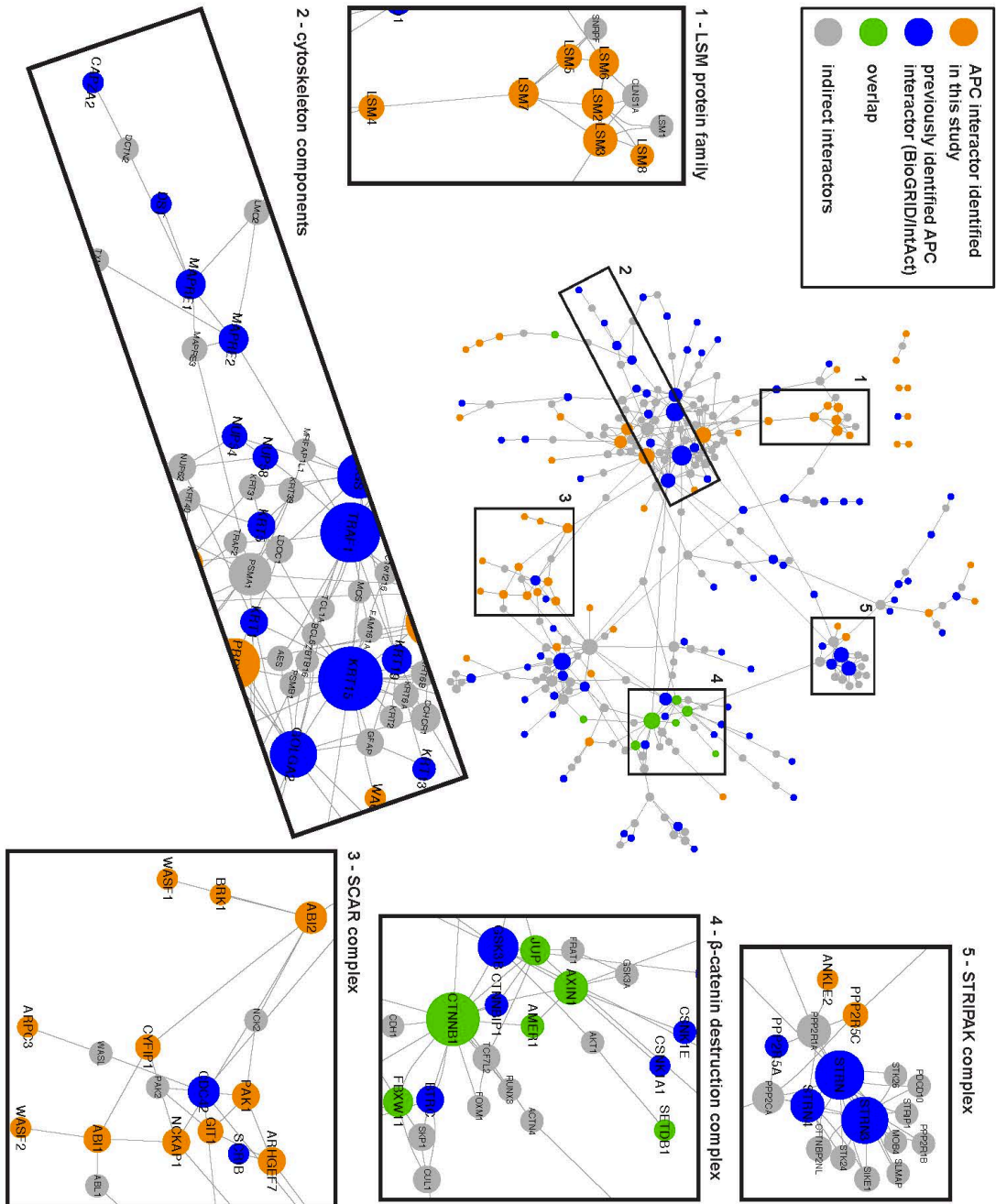
918 replicates/condition. Significance determined by two-way ANOVA followed by Sidak's
919 multiple comparison test; p value: *** < 0.0003. **E** MTT proliferation assay in Colo320
920 cells treated with siRNA against β -catenin or MINK1. Shown is the mean absorbance
921 from triplicate measurements. Significance relative to control determined by one-way
922 ANOVA followed by Dunnett's multiple comparison test, p value: * < 0.05, ** < 0.01.
923

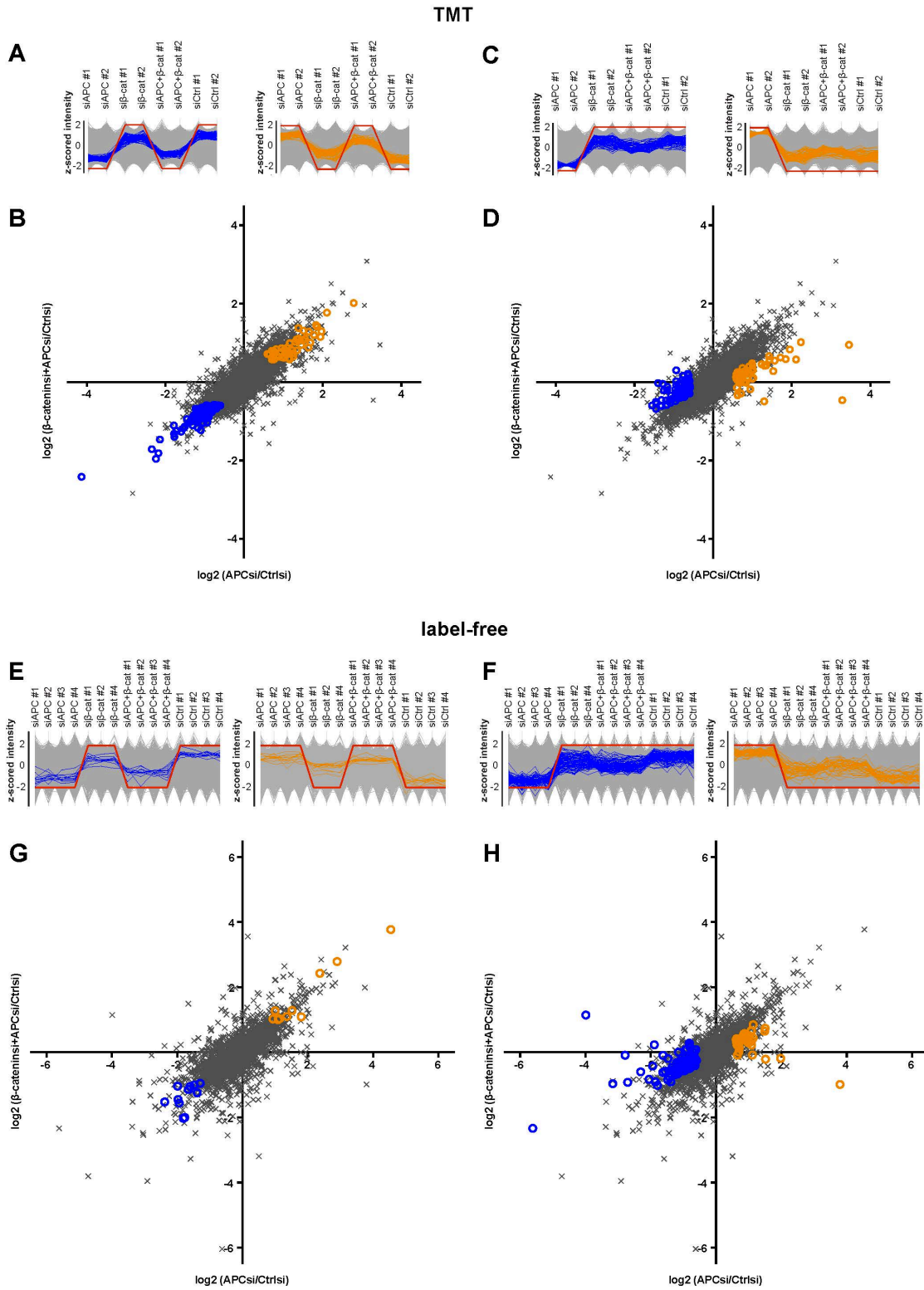
924 **Figures**

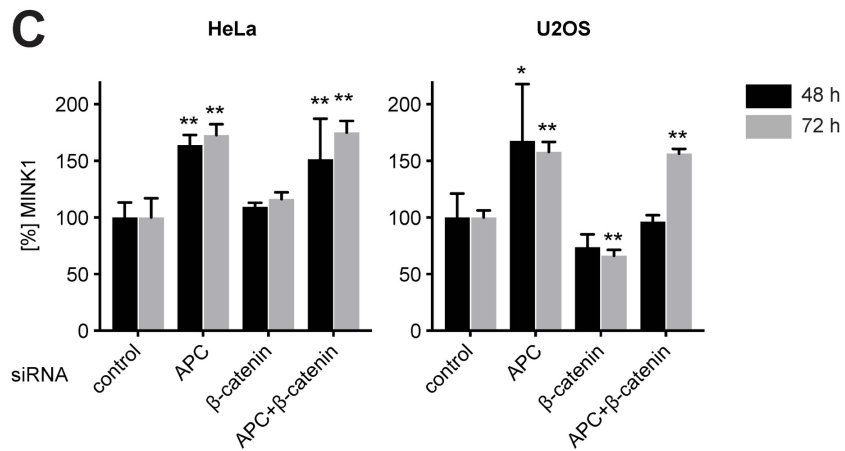
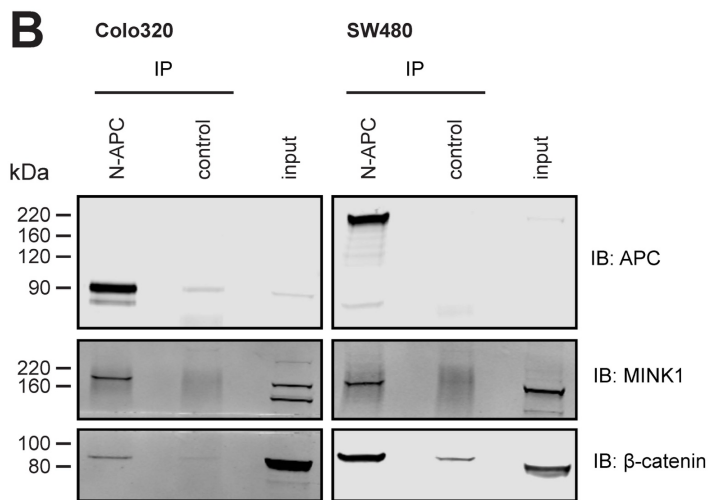
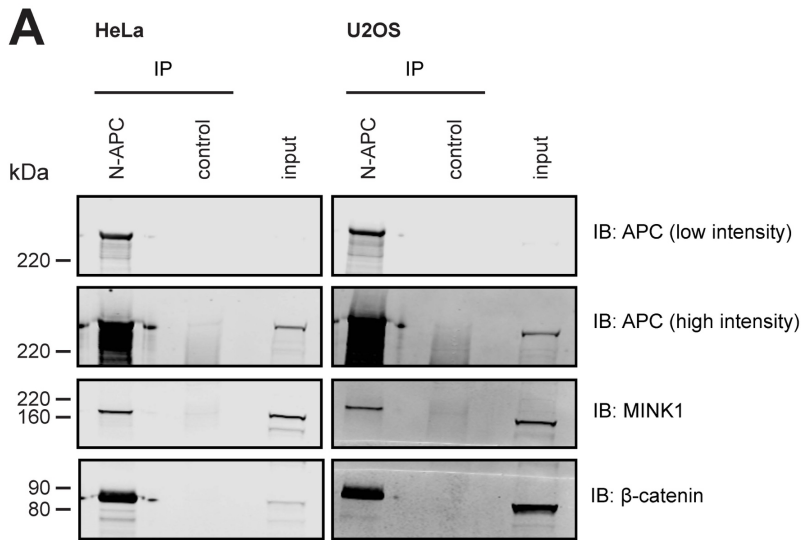
925 **Figure 1**

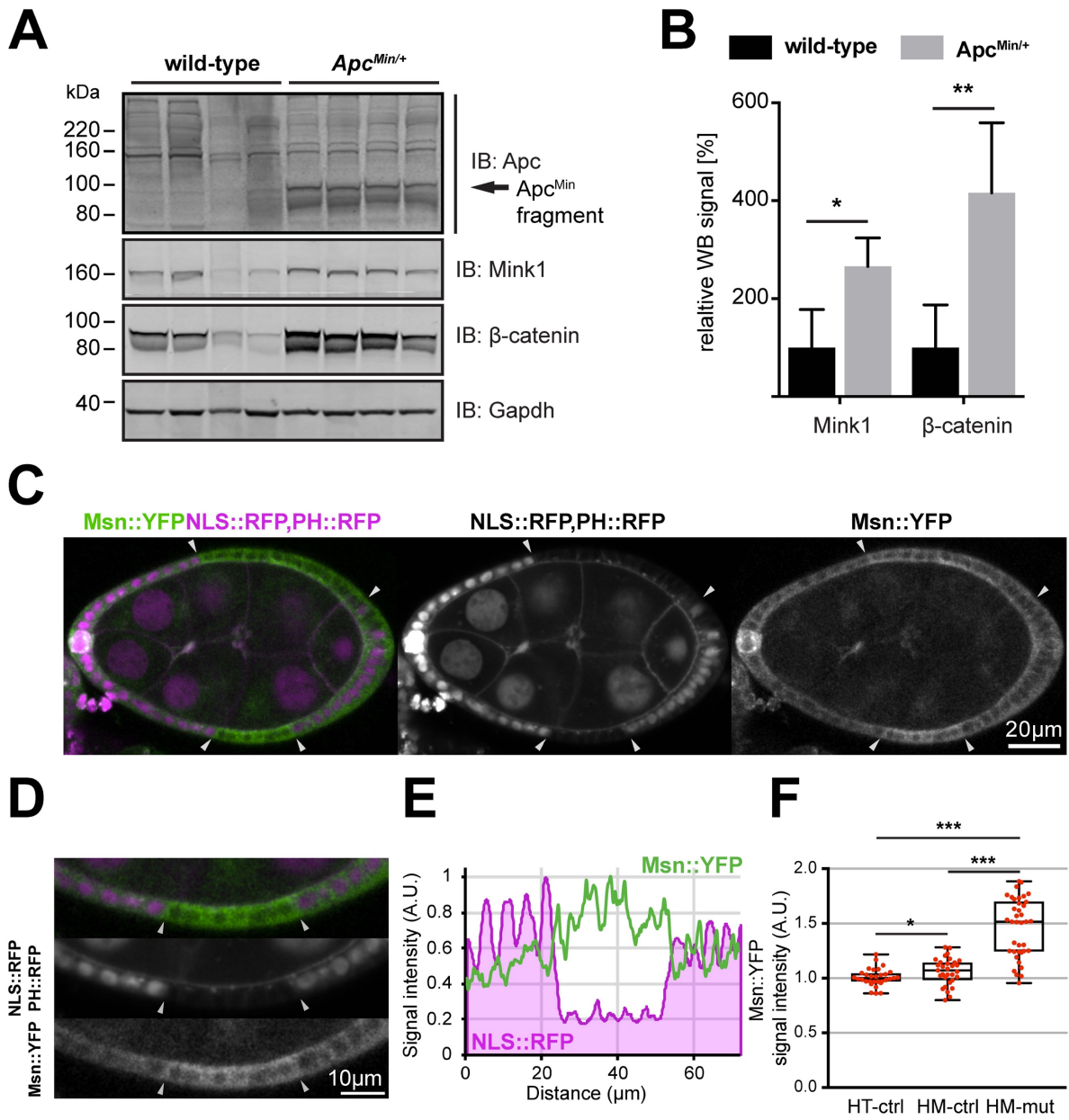


926









933

934

